Available online at www.sciencedirect.com
ScienceDirect
International Journal of Thermal Sciences 47 (2008) 1571–1586
International Journal of Thermal Sciences
www.elsevier.com/locate/ijts

Conjugate thermosolutal convection and condensation of humid air in cavities

N. Laaroussi, G. Lauriat *

Université Paris Est, Laboratoire de Modelisation et Simulation Multiechelle, FRE 3160 CNRS, F-77454 Marne-la-Vallée cedex 2, France

Received 28 August 2007; received in revised form 23 November 2007; accepted 30 December 2007

Available online 20 February 2008

Abstract

Heat transfer by natural convection and surface condensation in two-dimensional enclosures in contact with a cold external ambient through a wall of finite thickness was studied numerically. Special attention was given on the modeling of the flow of a binary mixture consisting of humid air. Low-Mach number assumption was introduced in order to account for decreases in mixture mass and average pressure within the enclosure between the initial and steady states. The computations show that thermodynamic balances are satisfied within the accuracy of the numerical procedure. The heat and fluid flows with and without condensation are compared for various operating conditions. It is shown that vapor condensation increases the heat transfer rate at the cold wall at the early stage of the transient regime. The decrease in the average density of the mixture leads to significant variable's reductions at steady-state which, in turn, causes lower overall heat transfer rate than for dry air.

Keywords: Enclosure flows; Surface condensation; Natural convection; Conjugate heat transfer; Numerical heat transfer

1. Introduction

Combined buoyancy forces of heat and mass transfer resulting from temperature and concentration gradients were shown to have large influences on heat transfer of fluid mixtures in many engineering systems, drying processes and building technology, for example. Natural convection of binary mixtures enclosed in a cavity was widely studied. Comprehensive reviews can be found, for example, in Weaver and Viskanta [1,2] or in the textbooks by Gebhart et al. [3] and Bejan [4]. However, most of the natural convection works due to combined thermal and mass driving buoyancy forces considered uniform temperature and concentration field at the walls, or heat flux boundary conditions (Dirichlet or Neumann formulations) and, no-slip velocity conditions. The Boussinesq approximation was largely used in conjunction with various non-dimensionalizations of the conservation equations. In a number of studies published in the current literature, the authors focused on the influences of flow parameters such as the mass and thermal Grashof numbers, Prandtl and Schmidt (or Lewis) numbers. Many numerical works which addressed cavity problems were on different combination of the driving forces (aiding or opposing according to the sign of the buoyancy parameter) and orientation of the enclosure with respect to the gravity vector. Unfortunately, many cases solved numerically are fully unrealistic because fluids and enclosures corresponding to these dimensionless parameters do not yet exist. For example, crystal growth by chemical vapor deposition and vapor deposition of thin films stand largely out of the domain of validity of the assumptions introduced in many of the flow models used.

In a large variety of applications, a condensable species A is the component of a binary mixture with the carrier gas B not soluble in A. This is the case of humid air which can be considered as an ideal gas mixture of dry air and water vapor. In this study, we considered condensation of water vapor in a cavity through investigations of cases for which experiments could be easily conducted. In order to restrict the numerical predictions to the laminar flow regime (available turbulence models still introduce non-well based constants or numerical incertainties for thermosolutal cavity flows), the size of the cavity must be quite small. Significant condensation effects on the surfaces occur indeed with rather large temperature differences and/or

* Corresponding author. Tel.: +33 1 60 95 72 69; fax: +33 1 60 95 72 94.
E-mail address: lauriat@univ-mlv.fr (G. Lauriat).

1290-0729/$ – see front matter
doi:10.1016/j.ijthermalsci.2007.12.014

Nomenclature

a	thermal diffusivity	$m^2\,s^{-1}$
A	enclosure aspect ratio, $= H/D$	
C_p	specific heat	$J\,K^{-1}\,kg^{-1}$
D	cavity width	m
$D_{v,m}$	binary mass diffusion coefficient	$m^2\,s^{-1}$
e	thickness of the bounding wall	m
g	gravitational acceleration	$m\,s^{-2}$
h	enthalpy	$J\,kg^{-1}$
$\overline{h}$	mixture enthalpy	$J\,kg^{-1}$
h_{lv}	latent heat	$J\,kg^{-1}$
h_{cv}	convective heat transfer coefficient	$W\,m^{-2}\,K^{-1}$
H	cavity height	m
$\overline{\overline{I}}$	unit tensor	
k	thermal conductivity	$W\,m^{-1}\,K^{-1}$
m_{cond}	mass of water vapor condensed per unit length	$kg\,m^{-1}$
$\dot{m}_{\mathrm{cond}}$	mass flow rate of water vapor condensed per unit length	$kg\,s^{-1}\,m^{-1}$
M	molecular weight	
N	buoyancy parameter, $N = Ra_M/Ra_T$	
$\overline{Nu}$	average Nusselt number based on cavity width	
p	pressure	Pa
p_{vs}	saturation pressure of vapor	Pa
Pr	mixture Prandtl number, $= \nu_m/a_m$	
q_w	cold wall heat flux density	$W\,m^{-2}$
R	universal gas constant, $= 8.315\ kJ\,kmol^{-1}\,K^{-1}$	
Ra_M	effective solutal Rayleigh number, $Ra_M = \rho_m g\beta_M(\overline{W}_h - \overline{W}_c)D^3/\mu_m a_m$	
Ra_T	effective thermal Rayleigh number, $Ra_T = \rho_m g\beta_T(\overline{T}_h - \overline{T}_c)D^3/\mu_m a_m$	
t	time	s
T	temperature	K
$\vec{V} = (u, v)$	velocity vector	$m\,s^{-1}$
W	mass fraction	
(x, y)	coordinates	m

Greek symbols

β_M	solutal coefficient of volumetric expansion	
β_T	thermal coefficient of volumetric expansion	K^{-1}
ΔT	temperature difference, $= (T_h - T_\infty)$ or $(T_0 - T_\infty)$	K
μ_m	dynamic viscosity of humid air	$N\,m^{-1}\,s^{-1}$
ϕ	relative humidity	%
Ψ	streamfunction	
ρ	density	$kg\,m^{-3}$
$\overline{\overline{\tau}}$	viscous stress tensor	
ξ	stretching parameter	

Subscripts

a	dry air
cond	condensation
dp	dew point
h	hot wall
m	mixture
0	initial condition
s	solid wall
S	solutal
T	thermal
v	vapor
w, i	interfacial quantity
∞	ambient fluid

Superscript

$-$	average quantity

large mass fraction differences within the cavity since the Lewis number of water vapor is close to unity.

Considerable research was conducted during the last decades on buoyancy-induced heat and mass transfer over flat surfaces of different slopes for both transient and steady flows. However, in the majority of these studies, as underlined by Rahman and Lampinen [5], the normal interface velocity component due to the concentration gradient at the surfaces was neglected. The importance of the interface velocity was considered in the study of Chang and Lin [6] for thermosolutal convection from a vertical plate and by Lin et al. [7] for vaporization of a thin liquid water film on a vertical tube wall in laminar mixed convection flows. Yan et al. [8] examined vaporization or condensation of water vapor in the case of mixed convection flows between parallel plates for various heating conditions, and a particular attention was paid to the investigation of the transport of latent heat. More recently, Lee et al. [9] investigated mixed convection in vertical rectangular ducts and Desrayaud and Lauriat [10] considered laminar natural convection of humid air in a vertical channel with cold, isothermal wetted walls. Since an elliptical, but incompressible, formulation was retained in this last study, it was possible to investigate the change in the flow from the developing regime to the single-plate regime.

Thermosolutal convection associated with evaporation of thin liquid water liquid films wetting the flat porous surfaces of a vertical channel was investigated by Yan et al. [11] by using an axially parabolic formulation in conjunction with the Boussinesq approximation. In this study, care was taken to satisfy the overall mass balance at every axial location. This constraint was used in the solution process to correctly guess the axial pressure gradient in the flow. The problem formulation was thus well-based. A similar porous-wall approach was used in Weaver and Viskanta [1,2] but for a much more complex cavity flow problem in which interdiffusion of species, variable thermophysical properties, Soret and Dufour effects were accounted for [2]. A rectangular enclosure in which a mass flux occurs at a hot vertical wall due to sublimation of a solid or evaporation of a liquid and condensation at the opposite cold wall was considered. The assumption of a binary mixture of ideal gases was invoked and normal velocities at the vertical walls were determined by a

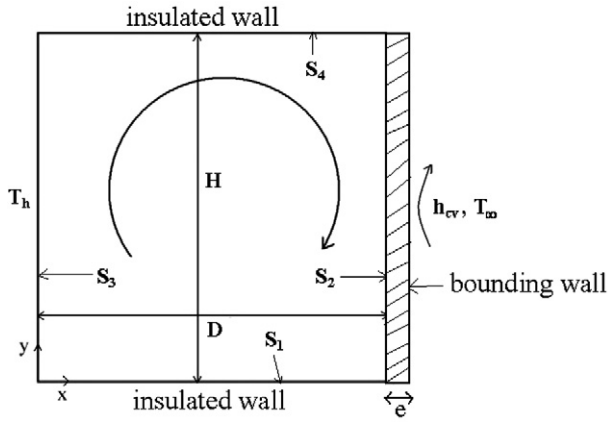

Fig. 1. Schematic diagram of the enclosure.

mass balance as in Yan et al. [11]. Since mass conservation within the cavity was assumed, the condensable species were introduced into and removed from the cavity at the hot and cold walls, respectively. An experimental set-up was built to check the numerical predictions (Weaver and Viskanta [12]). However, the comparisons showed only fair agreement for aiding flows and poor agreement for opposing flows. These discrepancies were attributed to the unsteady behaviors of the flows, not accounted for in the mathematical model. From our point of view, the large difficulties encountered in experimental set-up for controlling mass conservation and incompressible flow assumption could also explain such discrepancies.

We decided thus to follow a different procedure to model condensation processes in a closed cavity. Transient computations were first carried out between two equilibrium states, for which basic thermodynamic relationships were applied through hand calculations. To our best knowledge, the present study is the first using a transient, low-Mach number compressible formulation to model simultaneous heat and mass transfer by natural convection in cavities filled with humid air. However, it should be noted that condensation of water vapor in highly forced flow conditions around airfoil geometries were examined recently by Rusak and Lee [13], and by Karabelas and Markatos [14]. Compressible flow formulation, mixture two-phase model or nucleation and droplet growth models were used in these studies. As will be shown in the Result section, the non-Boussinesq, variable-properties, low-Mach-number compressible formulation appears to be the best approach for modeling significant mass transfer effects in humid air at constant volume.

2. Mathematical formulation

Consider a rectangular enclosure of width D and height H as shown in Fig. 1. One of the vertical wall is maintained at uniform hot temperature T_h and the opposite wall of finite thickness e and thermal conductivity k_s is in contact with a cold ambient at T_∞ with a uniform surface heat transfer coefficient h_{cv}. The two horizontal walls are adiabatic and impermeable. It is first assumed that the liquid films on the inside surfaces are extremely thin so that they can be treated as a boundary condition for heat and mass transfer as in Lin et al. [7] and in [10]. On account of the thermodynamic conditions considered in the present study, this assumption appears to be fully realistic since the volume of water condensed per surface unit is very small. However, even for a small amount of water vapor condensed, the incompressible assumption is not valid within a closed system. Therefore, a numerical procedure based on a finite volume method could not converge properly in the framework of this assumption since the global mass conservation of the mixture is not satisfied. Dufour and Soret effects are assumed negligibly small and there is no fog formation inside the cavity [15]. There are no chemical reactions, heat dissipation or heat generation, and the radiative heat transfer in the cavity is neglected. The flow is assumed two-dimensional and laminar. The continuity equation reads:

$$\frac{\partial \rho_m}{\partial t} + \nabla.(\rho_m \vec{V}) = 0 \tag{1}$$

The momentum equation is written as

$$\frac{\partial (\rho_m \vec{V})}{\partial t} + \nabla.(\rho_m \vec{V} \otimes \vec{V}) = -\nabla p' + \nabla.\bar{\bar{\tau}} + \rho_m \vec{g} \tag{2}$$

where p' is the fluctuating part of the static pressure decomposed as in [16]

$$p = \overline{P}(t) + p' \tag{3}$$

$\overline{P}$ is the average pressure (or thermodynamic pressure) such that $\overline{P} \gg p'$. The viscous stress tensor $\bar{\bar{\tau}}$ for a Newtonian fluid mixture is:

$$\bar{\bar{\tau}} = \mu_m \left[\nabla \vec{V} + (\nabla \vec{V})^T - \frac{2}{3}(\nabla.\vec{V})\bar{\bar{I}} \right] \tag{4}$$

For a binary mixture of ideal gases, the energy equation written in terms of enthalpy only is

$$\frac{\partial (\rho_m \bar{h})}{\partial t} + \nabla.(\rho_m \vec{V} \bar{h}) = \nabla.\left(\frac{k_m}{\overline{C}_p} \nabla \bar{h} \right) + \nabla.\left(\rho_m (h_v - h_a) D_{v,m} \nabla W_v \right) + \frac{\mathrm{d}\overline{P}}{\mathrm{d}t} \tag{5}$$

where $\bar{h}$ is the total enthalpy of the mixture, $\rho_m \bar{h} = \rho_v h_v + \rho_a h_a$, and $\mathrm{d}\bar{h} = \overline{C}_p \, \mathrm{d}T$. The second term of the right-hand side of the energy equation represents the contribution on the energy flux due to interdiffusion of species with air and water vapor having different enthalpies. The pressure term is for an ideal gas mixture and the assumption of negligible pressure fluctuations is invoked [17].

The mass species equation for the water vapor is

$$\frac{\partial (\rho_m W_v)}{\partial t} + \nabla.(\rho_m \vec{V} W_v) = \nabla.(\rho_m D_{v,m} \nabla W_v) \tag{6}$$

It should be mentioned that in the above equations all the thermophysical properties depend on the mixture temperature and concentration of each component. Since we are considering a perfect gas mixture, the dynamic viscosity, thermal conductivity and coefficient of thermal expansion of each component do not depend on pressure according to the kinetic theory. The variations of the thermophysical properties of dry air and pure water vapor with temperature as well as the mixture properties

are calculated by the formulae given by Fujii et al. [18] (see also Lin et al. [7]).

The system of conservation equations is thus completed by the ideal gas law used for the calculations of the mixture density field:

$$\overline{P} = \rho_m RT\left(\frac{W_v}{M_v} + \frac{W_a}{M_a}\right) \tag{7}$$

It is worth noting that the flow quantities in Eq. (7) vary with time. The pressure decomposition (Eq. (3)) requires the introduction of an additional equation to recover the average pressure. It can be done by writing an overall mass balance equation which takes into account the mass of water vapor condensed at the walls (i.e. the mass of the mixture flowing out of the domain of computation). From the equation of state, it can be readily shown that

$$\int_V \frac{\rho_m}{\overline{P}}\frac{\mathrm{d}\overline{P}}{\mathrm{d}t}\,\mathrm{d}V = \int_V \frac{\partial \rho_m}{\partial t}\,\mathrm{d}V + \int_V \frac{\rho_m}{T}\frac{\partial T}{\partial t}\,\mathrm{d}V \tag{8}$$

where the first term of the RHS stands for the loss of mixture mass denoted in what follows as $\dot{m}_{\mathrm{cond}}$. Therefore Eq. (8) can be expressed as

$$\frac{\overline{\rho}_m V}{\overline{P}}\frac{\mathrm{d}\overline{P}}{\mathrm{d}t} = \dot{m}_{\mathrm{cond}}(t) + \int_V \frac{\rho_m}{T}\frac{\partial T}{\partial t}\,\mathrm{d}V \tag{9}$$

In the vertical, cold bounding wall, the heat equation reads

$$\frac{\partial T_s}{\partial t} = a_s \nabla^2 T_s \tag{10}$$

2.1. Boundary conditions

For the parts of the bounding walls which are at a temperature lower than the dew-point temperature, vapor condensation rate produces a normal velocity of vapor which is calculated from the expression of the interfacial mass flux given by Fick's law. The following expression of the normal velocity component at liquid-mixture interface along wall i assumes that the solubility of air in water is negligibly small and that the liquid film is stationary:

$$\begin{cases} \vec{V}.\vec{t}_{\,i} = 0, \quad \vec{V}.\vec{n}_{\,i} = -\dfrac{D_{v,m}}{(1-W_{v,i})}\dfrac{\partial W_v}{\partial n_i} \\ \qquad\qquad \text{if } p_v(T_{w,i}) \geqslant p_{vs}(T_{w,i}) \\ \vec{V} = 0 \quad \text{otherwise} \end{cases} \tag{11}$$

where $\vec{t}_{\,i}$ denotes the tangent vector along the interface, $\partial/\partial n_i$ the gradient in the direction of the outward normal $\vec{n}_{\,i}$ to the interface and, $p_{vs}(T_{w,i})$ the saturation pressure at $T_{w,i}$. By assuming that the humid air–liquid water film interface is in thermodynamic equilibrium, the interfacial mass fraction of water vapor is related to the partial pressure of the water vapor at saturation condition through the equation

$$W_{v,i} = \frac{M_v p_v(T_{w,i})}{[M_v p_v(T_{w,i}) + M_a(p - p_v(T_{w,i}))]} \tag{12}$$

where $p_v(T_{w,i})$ is the partial pressure of water vapor at the wall temperature. When accounting for sensible heat transfer, species interdiffusion flux and latent heat transfer due to the rate of mass transfer, the total heat fluxes at the cold and adiabatic walls are:

$$\begin{cases} q_w = -k_m\dfrac{\partial T_m}{\partial n_i} - (h_v - h_a)\rho_m D_{v,m}\dfrac{\partial W_v}{\partial n_i} \\ \qquad + \dfrac{\rho_m D_{v,m} h_{lv}}{(1-W_{v,i})}\dfrac{\partial W_v}{\partial n_i} \\ \qquad\qquad \text{if } p_v(T_{w,i}) \geqslant p_{vs}(T_{w,i}) \\ q_w = -k_m\dfrac{\partial T_m}{\partial n_i} \quad \text{otherwise} \end{cases} \tag{13}$$

where $q_w = -k_s \partial T_s/\partial x|_D$ at the inner bounding wall surface and $q_w = 0$ along the horizontal adiabatic walls, at which the diffusive energy heat flux is counterbalanced by the energy flux due to species interdiffusion and latent heat flux.

At the hot wall

$$T = T_h \quad \text{at } x = 0, \forall y \tag{14}$$

Along the surface of the bounding wall surface in contact with the cold ambient at T_∞

$$-k_s\frac{\partial T_s}{\partial x} = h_{cv}(T_s - T_\infty) \quad \text{at } x = D + e, \forall y \tag{15}$$

where h_{cv} is the surface heat transfer coefficient assumed to be uniform along the wall.

The transport equation for water vapor is subjected to the following boundary conditions

$$\begin{cases} W_v = \dfrac{M_v p_v(T_{w,i})}{[M_v p_v(T_{w,i}) + M_a(p - p_v(T_{w,i}))]} \\ \qquad\qquad \text{if } p_v(T_{w,i}) \geqslant p_{vs}(T_{w,i}) \\ \dfrac{\partial W_v}{\partial n_i} = 0 \quad \text{otherwise} \end{cases} \tag{16}$$

2.2. Mass and heat flux balances

As already mentioned, the total mass of the mixture decreases with time until steady state. The mass difference between times t_1 and t_2 equals the mass of water condensed along the parts of the walls where the temperature is below the dew-point temperature. The mass balance can be written as

$$\int_v \rho_m(x,y,t_2)\,\mathrm{d}v - \int_v \rho_m(x,y,t_1)\,\mathrm{d}v = -\sum_i \int_{t_1}^{t_2}\int_{S_i} \frac{\rho_m D_{v,m}}{(1-W_{v,i})}\frac{\partial W_v}{\partial n_i}\bigg|_w \mathrm{d}S_i\,\mathrm{d}t \tag{17}$$

In the transient regime, the following heat flux balance must be achieved

$$-\int_0^H k_s\frac{\partial T_s(x,y,t)}{\partial x}\bigg|_{x=D}\mathrm{d}y = -\int_0^H k_m\frac{\partial T_m(x,y,t)}{\partial x}\bigg|_{x=D}\mathrm{d}y$$

$$-\int_0^H (h_v - h_a)\rho_m D_{v,m} \frac{\partial W_v(x,y,t)}{\partial x}\bigg|_{x=D} \mathrm{d}y + \int_0^H h_{lv} \frac{\rho_m D_{v,m}}{(1-W_{v,i})} \frac{\partial W_v(x,y,t)}{\partial x}\bigg|_{x=D} \mathrm{d}y \tag{18}$$

For water–vapor condensation and in the framework of the present study, the second term of the RHS is obviously very small. The main interest here is in the relative importance of the sensible and latent heat fluxes.

It should be noted that condensation does not occur at steady state since the water vapor is then in thermodynamic equilibrium with the wet surfaces. Therefore the above heat flux balance becomes at steady state ($\partial W_v/\partial n_i = 0$):

$$h_{cv}\int_0^H \big(T_s(D+e,y) - T_\infty\big)\,\mathrm{d}y = -\int_0^H k_m \frac{\partial T_m(x,y)}{\partial x}\bigg|_{x=D} \mathrm{d}y \tag{19}$$

3. Solution method

Calculations were carried-out using the control volume code Fluent 6.2 (Fluent Inc. [19]). Results of the simulations were collected and processed employing in-house software. A second-order upwind scheme was used for the advective and transport terms. The velocity-pressure coupling was solved with the PISO algorithm and the pressure was calculated with a body-force weighted scheme (Fluent 6.2 User's Guide, n.d.). The governing equations were solved sequentially with a decoupled implicit scheme. The transient calculations were achieved using an iterative time advancement scheme. The time step was chosen such that the Courant–Friedrichs–Lewy (CFL) condition was satisfied for all of the cases (CFL $\leqslant 1$) [20]. Since imposition of the above boundary conditions is not available, the mass and heat fluxes at the boundaries were retrieved through extensive use of user-defined functions (UDFs) called at each time step. Source terms were introduced only in the cells adjacent to the walls in the mass (mixture and species) and energy conservation equations to account for the loss of mass within the cavity and increase of the heat flux due to condensation of water vapor at the walls. The source term put in the mass conservation equations was

$$\begin{cases} S_m = \dot{m}_v \times \dfrac{A_G}{V_G} = -\dfrac{\rho_m D_{v,m}}{(1-W_{v,i})} \dfrac{\partial W_v}{\partial n_i} \times \dfrac{A_G}{V_G} \\ \qquad \text{if } p_v(T_{w,i}) \geqslant p_{vs}(T_{w,i}) \\ S_m = 0 \quad \text{otherwise} \end{cases} \tag{20}$$

where A_G and V_G are the surface and volume of the cell where the source term is introduced. Similarly, a source term $S_v = S_m$ was added in the mass conservation equation for water vapor. A source term $S_h = \dot{m}_v h_{lv}$ was also introduced in the energy equation to model the latent heat flux at the walls.

The solution procedure is outlined below:

(1) Specify uniform initial conditions.
(2) Calculations of the mixture thermophysical properties.
(3) Calculations of the source terms.
(4) Integrate sequentially the system of governing equations.
(5) Check of the overall conservation of mass.
(6) Steps (2)–(4) are applied successively until steady state is reached.

The calculation domain was mapped with rectangular structured grids refined close to the walls. Validations of the source term strategy and non-Boussinesq model available in the computer code were carried out by considering three test cases. A comparison with a recently published benchmark study [17, 21] was first conducted. We investigated then the transient evolutions of mixtures enclosed within two kind of square cavities, initially at uniform temperature and mass fraction, which are suddenly cooled at a temperature level below the dew-point temperature.

In the comparison case, large temperature difference was applied between the vertical isothermal walls of a square, differentially heated cavity initially filled with dry air at atmospheric pressure and at temperature $T_0 = 600$ K equal to the average $(T_c + T_h)/2$. The specific heat at constant pressure and Prandtl number were assumed constant ($Pr_0 = 0.71$) for the temperature differences considered while the dynamic viscosity and thermal conductivity were allowed to vary according to Sutherland's law [17]. In the present paper, comparisons with the benchmark data [21] are shown for the large temperature difference $\Delta T = 1.2T_0$ and for two Rayleigh numbers based on thermophysical properties at T_0, $Ra_0 = 10^6$ and 10^7, respectively. Two non-uniform meshes of 100×100 and 200×200 were used for the computations.

The compressible results do not exhibit the centrosymmetry property associated with the Boussinesq approximation: horizontal velocities along the top adiabatic wall are higher than those along the bottom wall and, the thermal boundary layer thickness along the cold wall is thinner than that along the hot wall. Results obtained for constant as well as for temperature-dependent viscosity show that the changes in maximum vertical velocity components along the cold and hot walls agree with the increase in dynamic viscosity of a perfect gas with temperature. It should be noted that the decrease in thermodynamic pressure is about 15% when assuming constant viscosity and thermal conductivity and only 8% for variable properties. Such small pressure reductions may be explained by the choice of the initial conditions suggested in the benchmark problem for low Mach number solvers [17]. The data reported in Table 1 show that the maximum differences between the present results for the 200×200 mesh and the most accurate solution provided in [21] for the average Nusselt number is within 0.15% for the two Rayleigh numbers considered.

Steady-state solutions for natural convection in a differentially heated cavity do not depend on the initial conditions when the Boussinesq approximation with constant thermophysical properties is invoked. On the other hand, the fluid properties, especially the density, are temperature dependent for a given initial thermodynamic pressure. We thus reconsidered the above comparison exercise by using a much lower tem-

Table 1
Comparisons with benchmark solutions [21] for a differentially heated square cavity with $Ra_0 = 10^6$, $Ra_0 = 10^7$ and $\Delta T = 1.2T_0$ for variable thermal properties ($y* = y/H$, $x* = x/D$, min, max: minimal and maximal values, $P_0 = 101325$ Pa)

Ra	10^6	10^6	[21]	10^7	10^7	[21]
Mesh	100×100	200×200	2048×2048	100×100	200×200	2048×2048
ξ	1.05	1.05		1.05	1.05	
$\Delta t\,(s)$	0.01	0.005		0.01	0.005	
Nu_h	8.6839	8.6998	8.6866	16.2975	16.2589	16.2410
Nu_c	8.6839	8.6998	8.6866	16.2975	16.2589	16.2410
$Nu(0, 0.5)$	7.6746	7.5606	7.4593	13.5937	13.3979	13.189
$Nu(1, 0.5)$	8.4767	8.5495	8.6372	15.2154	15.3721	15.512
$\max_y(Nu(0, y^*))$	20.3164	20.2887	20.2704	46.7616	46.5065	46.379
$\min_y(Nu(0, y^*))$	1.0677	1.0671	1.0677	1.4588	1.4545	1.454
$\max_y(Nu(1, y^*))$	15.6234	15.5446	15.5194	34.7010	34.5540	34.272
$\min_y(Nu(1, y^*))$	0.7579	0.7578	0.7575	1.09358	1.0872	1.089
$\overline{P}/P_0$	0.924077	0.924745	0.924489	0.92170	0.92263	0.92264

Table 2
Comparison between steady-state quantities for dry air (constant thermophysical properties at $T_0 = 315$ K, except density)

Initial conditions	$T_0 = 315$ K	$T_0 = 350$ K	$T_0 = 280$ K	$T_0 = 315$ K
Model	Boussinesq	compressible	compressible	compressible
$\overline{\rho}_m$ (kg m^{-3})	1.12	1.0086	1.26	1.12
$\overline{P}$ (N m^{-2})				
at $t = 0$	101,325	101,325	101,325	101,325
at $t = \infty$	101,325	91,393	113,197	100,941
$\overline{q}_w$ (W m^{-2})	268.59	244.65	286.29	268.79
$\overline{Nu}$	14.22	12.94	15.15	14.22
Ra	$5.53 \cdot 10^6$	$4.48 \cdot 10^6$	$6.99 \cdot 10^6$	$5.53 \cdot 10^6$
$\overline{T}$ (K)	315	316.49	313.60	314.59

perature difference between the vertical walls while different initial conditions were applied. The geometry studied was a square cavity ($H = L = 0.1$ m) with uniform hot and cold wall temperatures of $T_h = 350$ K and $T_c = 280$ K. The thermophysical properties were assumed constant (dry air at a reference temperature $T_r = 315$ K equal to the average $(T_c + T_h)/2$), except the density for compressible computations. The cavity was initially filled with quiescent dry air at atmospheric pressure ($\overline{P}(0) = 101{,}325$ Pa). Three initial uniform fluid temperatures were considered for the non-Boussinesq formulation: $T_0 = 280$ K, $T_0 = 315$ K and $T_0 = 350$ K. Obviously, mass conservation implies constant volume average density for both formulations. On the other hand, thermodynamic pressure $\overline{P}$ and, thus volume averaged fluid temperature $\overline{T} = \overline{P}/r\overline{\rho}$ may increase or decrease between initial and steady states according to the value of the initial fluid temperature when a compressible approach is applied. The results reported in Table 2 show that the compressible and Boussinesq computations yield almost equal overall quantities provided that $T_0 = 315$ K although density distribution $\rho(x, y)$ lies in the range [1.0086, 1.26] for the compressible solution. On the other hand, Table 2 clearly shows that the steady-state solution is initial-temperature dependent, despite the rather small temperature difference considered (70 K).

A grid refinement study and changes in the time step were conducted in the case of transient thermosolutal convection

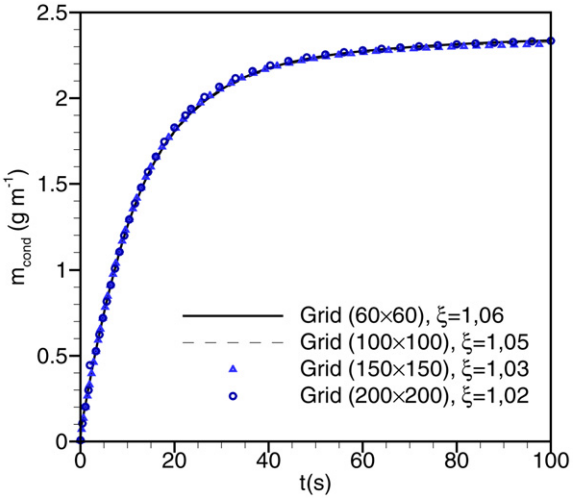

Fig. 2. Time-evolution of the mass of water vapor condensed for different computational grids.

Table 3
Time step study: mass of water vapor condensed (g m^{-1}) at various times during the evolution of condensation

Δt (s)	10^{-3}	$8 \cdot 10^{-4}$	$6 \cdot 10^{-4}$	$4 \cdot 10^{-4}$	$2 \cdot 10^{-4}$
$t = 10$ s	1.244	1.256	1.260	1.271	1.273
$t = 15$ s	1.580	1.593	1.600	1.607	1.608
$t = 20$ s	1.796	1.818	1.821	1.824	1.827
$t = 30$ s	2.068	2.066	2.067	2.070	2.072

in a square cavity. Four different grid distributions have been tested. Comparison of the evolution of the mass of water vapor condensed at the walls displayed in Fig. 2 shows that the solutions calculated on the four grids are very close. In view of these results, a 100×100 non-uniform grid was adopted. Time step was then varied to ensure that the transient evolution was accurately predicted, especially at the beginning of condensation. The amount of mass of water vapor condensed at different times are presented in Table 3 according to the time step used. Comparisons of these results from $\Delta t = 2 \cdot 10^{-4}$ s and $\Delta t = 4 \cdot 10^{-4}$ s show differences less than 0.5%. For that reason, calculation were performed by using $\Delta t = 4 \cdot 10^{-4}$ s. It should be noted that the maximum value of the CFL number in

Table 4
Thermodynamic properties of the mixture at $t = 0$ and at steady-state

T_0 (K)	ϕ_0	$t = 0$	$t = \infty$	m_{cond}
293	80%	$\rho_m = 1.1964\ \text{kg m}^{-3}$ $W_v = 0.0115$ $P_0 = 101{,}325\ \text{Pa}$ $P_v = 1861\ \text{Pa}$ $m_v = 0.55\ \text{g m}^{-1}$	$\rho_m = 1.1901\ \text{kg m}^{-3}$ $W_v = 0.0063$ $P_\infty = 96{,}029\ \text{Pa}$ $P_v = 990\ \text{Pa}$ $m_v = 0.3\ \text{g m}^{-1}$	$0.25\ \text{g m}^{-1}$
350	50%	$\rho_m = 0.93\ \text{kg m}^{-3}$ $W_v = 0.138$ $P_0 = 101{,}325\ \text{Pa}$ $P_v = 20{,}760\ \text{Pa}$ $m_v = 5.14\ \text{g m}^{-1}$	$\rho_m = 0.809\ \text{kg m}^{-3}$ $W_v = 0.0095$ $P_\infty = 65{,}156\ \text{Pa}$ $P_v = 990\ \text{Pa}$ $m_v = 0.3\ \text{g m}^{-1}$	$4.84\ \text{g m}^{-1}$

the flow field was CFL = 0.17 in that case and for a 100×100 non-uniform grid.

4. Results

4.1. Transient thermosolutal convection in a square cavity

A 0.2 m × 0.2 m square cavity initially filled with moist air at atmospheric pressure, temperature T_0 and relative humidity ϕ_0 was first investigated. At $t > 0$, the two vertical walls with zero thickness ($e = 0$) were uniformly cooled at $T_c = 280$ K while the horizontal walls were adiabatic. The wall temperatures were such that water vapor started to condense at the two vertical walls and then at the adiabatic walls. According to the temperature difference $T_0 - T_c$, a strong thermosolutal flow may occur at early times and then becomes weaker to end in a purely diffusive regime. Obviously, the steady state is a saturated mixture in thermodynamic equilibrium at T_c with zero interfacial mass transfer and 100% relative humidity everywhere.

Two sets of initial conditions were investigated: $T_0 = 293$ K and $\phi_0 = 80\%$, $T_0 = 350$ K and $\phi_0 = 50\%$. The humid air properties for these two combinations of T_0 and ϕ_0 are reported in Table 4. For both initial conditions, thermal buoyancy forces dominate mass buoyancy forces at the beginning of the transient regime. The exact values of the mass of water vapor condensed at the four walls at steady state (calculated from the first thermodynamic principle) are $m_{\text{cond}} = 0.25\ \text{g m}^{-1}$ and $m_{\text{cond}} = 4.84\ \text{g m}^{-1}$ for the first and second combinations of T_0 and ϕ_0, respectively. These amounts of liquid water can be compared to the mixture mass at initial conditions: $m_m \simeq 48.86\ \text{g m}^{-1}$ and $m_m \simeq 37.2\ \text{g m}^{-1}$, respectively. The first case could be solved quite accurately within the framework of the Boussinesq approximation, unlike the second one due to the temperature differences at the beginning of the transient evolution ($\Delta T = 80$ K) and non-negligible loss of the mass of the gas mixture.

Thermal convection dominates for $T_0 = 293$ K and $\phi_0 = 80\%$ since $Ra_{T,\max}/Ra_{M,\max} \simeq 14$ (the maximum effective Rayleigh numbers being here based on the mixture properties at T_0 and on the differences in temperatures and mass fractions between the initial and steady-state conditions). For $T_0 = 350$ K and $\phi_0 = 50\%$, $Ra_{T,\max}/Ra_{M,\max} \simeq 2.8$ and the thermal and solutal effects are of the same order of magnitude. A rough estimate of the sum $(Ra_{T,\max} + Ra_{M,\max})$ shows also that its value lies between 10^6 and 10^7 at the early times. Therefore, the laminar assumption holds.

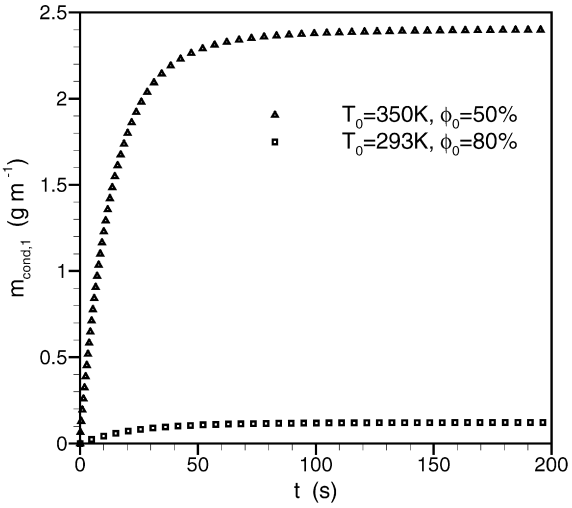

Fig. 3. Time-evolution of the mass of water vapor condensed at one of the vertical cold walls for both vertical walls at the same temperature and with zero thickness ($e = 0$).

The mass of water vapor condensed at the four walls at time t was calculated from the following relationship:

$$m_{\text{cond}}(t) = \int_S \left.\frac{\mathrm{d}m_{\text{v,cond}}}{\mathrm{d}t}\right|_w \mathrm{d}t = \int_0^t \int_S \frac{\rho_m D_{v,m}}{(W_v - 1)} \left.\frac{\partial W_v}{\partial n}\right|_w \mathrm{d}S\,\mathrm{d}t \tag{21}$$

where S is the total area of the four cavity surfaces. At steady state ($t \to \infty$), Eq. (21) must match the mass balance

$$m_{\text{cond}} = (\overline{\rho}_{m,t=\infty} - \overline{\rho}_{m,t=0})V \tag{22}$$

Fig. 3 shows the time-evolutions of the mass of water vapor condensed at one of the vertical walls for the two cases studied. Obviously, the length of the transient regime is higher for $T_0 = 350$ K and $\phi_0 = 50\%$. The solutal effect becomes very small when m_{cond} reaches a plateau, i.e. $t \approx 30$ s and $t \approx 60$ s for $T_0 = 293$ K and $T_0 = 350$ K, respectively. The values of the mass condensed at the four walls match the thermodynamic predictions within 0.1%. Fig. 3 indicates that most of water vapor condenses at the cold vertical walls. In addition, since the thermal and buoyancy forces act in the same direction, the mass of water vapor condensed at the bottom adiabatic wall is lower than at the top wall. The time-decrease in the mean mixture pressure is plotted in Fig. 4: as expected, $\overline{P}$ tends towards the thermodynamic values reported in Table 4. The mean density follows similar variations since the mixture is assumed to be a perfect gas at constant volume.

4.2. Conjugate transient thermosolutal convection in a square cavity

The above configuration is not well appropriate for checking the overall energy balance, at least from a computational point

of view. Therefore, we considered then a more realistic problem for which the cooled vertical sides of a 0.2 m × 0.2 m square cavity were two identical walls of finite thickness e and thermal conductivities k_s. The walls were cooled from T_0 to the ambient temperature T_∞ with a uniform heat transfer coefficient at the vertical outside surfaces, h_{cv}. The initial mixture conditions were for a fluid at rest uniformly at $T_0 = 350$ K and $\phi_0 = 50\%$. The ambient temperature was kept at $T_\infty = 280$ K. The thermodynamic steady-state conditions and the mass of water vapor condensed must be identical to those calculated in the above section, whatever the values of h_{cv}, e and k_s are. The effect of the overall thermal conductance of the vertical walls is thus to modify the length of the transient regime, i.e the occurrences of thermal and solutal convection within the cavity.

The computations were carried out for aluminium side walls ($\rho_s = 2719$ kg m^{-3}, $C_{ps} = 900$ J kg^{-1} K^{-1}, $k_s = 200$ W m^{-1} K^{-1}) and two thicknesses were considered: $e = 1$ mm and $e = 3$ mm. The outside heat transfer coefficient was $h_{cv} = 25$ W m^{-2} K^{-1}. Therefore, the Biot number, $Bi = h_{cv}e/k_s$ was much lower than $Bi = 0.1$ so that a lumped system analysis shows that the horizontal temperature gradients in the walls become negligible within a short time following the initial state.

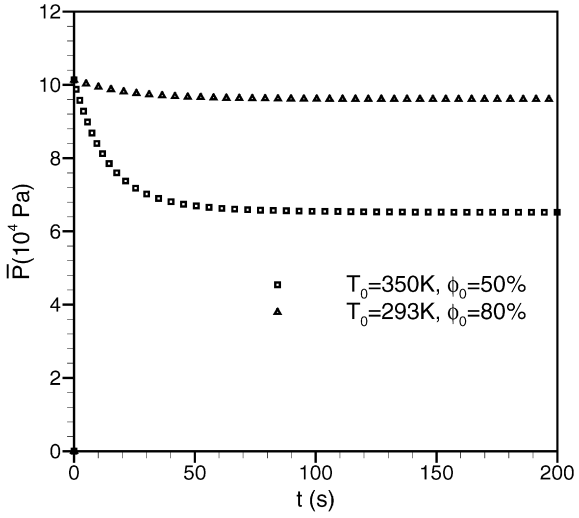

Fig. 4. Time-decrease in the mean mixture pressure for both vertical walls at the same temperature and with zero thickness ($e = 0$).

Fig. 5 shows the evolutions of the mass flow rate of water vapor condensed at the inner surfaces for the two bounding walls (S_1 and S_2 are for the vertical surfaces, S_3 and S_4 are for the bottom and top adiabatic walls, respectively). Due to the vertical symmetry of the problem about the center-plane of the cavity, the mass flow rates at S_1 and S_2 are the same while they are much lower at the adiabatic walls, especially at S_4 like for the configuration discussed above. Condensation starts as soon as the interior wall temperatures fall below the dew-point temperature ($T_{dp} \approx 330$ K), and then the process increases sharply up to a maximum value followed by a decrease to a zero value corresponding to the thermodynamic equilibrium. As expected, the time interval from $t = 0$ to the beginning of condensation at the vertical walls is very close to the one given by the thermal time constant deduced from the lumped capacitance method (i.e. $\Delta t \approx 30$ s and $\Delta t \approx 80$ s for $e = 1$ mm and $e = 3$ mm). Time integration of these curves leads to the same value of $m_{\text{cond}} = 4.84$ g m^{-1} as in the previous subsection. On the other hand, thermal convection starts immediately due to the low value of the Biot numbers for the two wall thicknesses as it can be seen in Fig. 6 showing the transient variations of the average heat flux densities at the walls.

At early times, the fluid motion is produced only by the temperature differences between the hot fluid in the cavity core and the cold fluid close to the vertical walls. The heat fluxes at the cold walls increase thus as fast as the inner surface wall temperatures decrease. When the lowest temperature at the vertical walls becomes less than T_{dp}, sharp increases in the heat fluxes are seen because of condensation. The changes in the slopes of the curves at $\Delta t \approx 27$ s for $e = 1$ mm and at $\Delta t \approx 81$ s for $e = 3$ mm indicate the beginning of condensation. On one hand, the thermal effects decrease because condensation produces increases in inner surface wall temperatures. On the other hand, solutal effects amplify according to the increase in solutal Rayleigh number. The peak in heat flux corresponds thus to the peak in condensation mass flow rate (Fig. 5). The length of the transient regime for $e = 3$ mm is about two times higher than

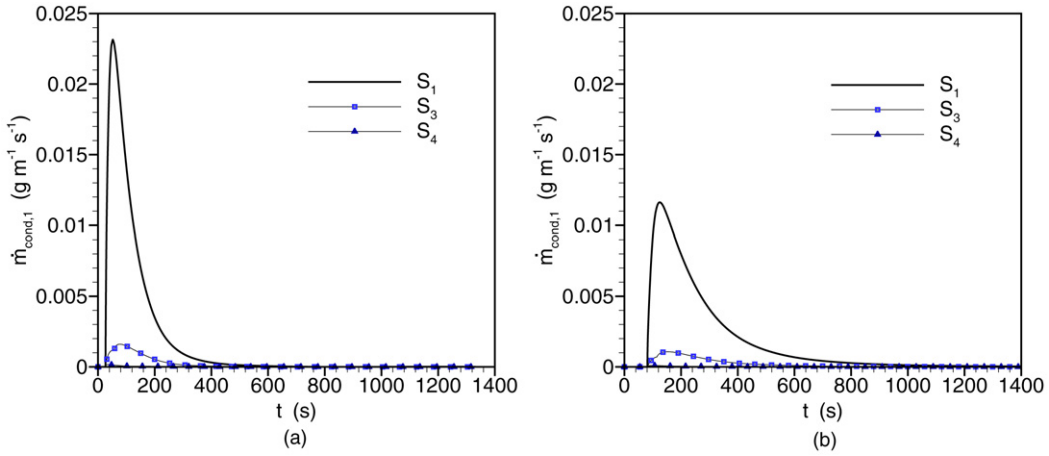

Fig. 5. Time variations of the mass flux condensed along the wall surfaces S_1, S_3 and S_4 for (a) $e = 1$ mm and (b) $e = 3$ mm.

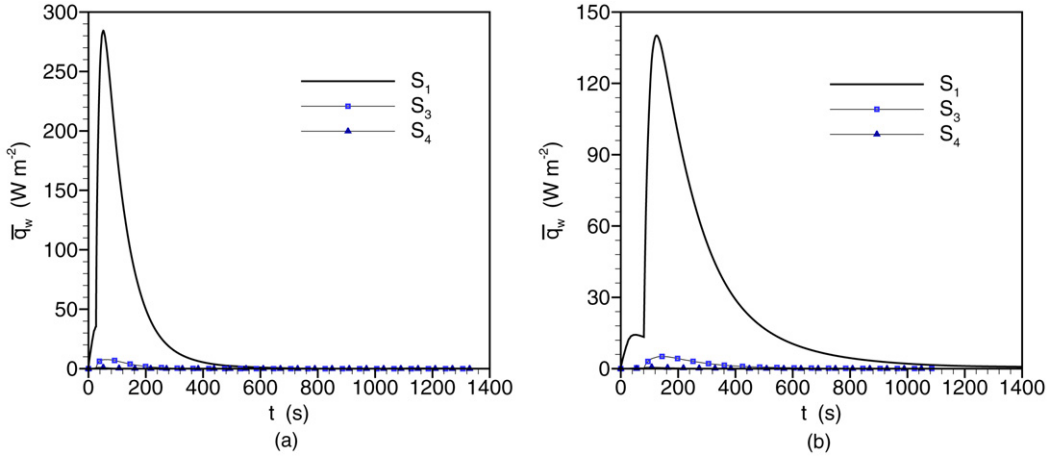

Fig. 6. Time variations of the averaged heat flux densities at S_1, S_3 and S_4 for (a) $e = 1$ mm and (b) $e = 3$ mm.

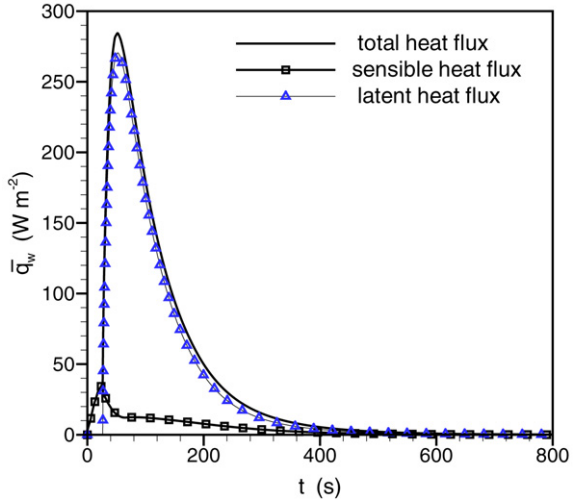

Fig. 7. Time variations of the total, sensible and latent heat fluxes at S_1 ($k_s = 200$ W/m K, $e = 1$ mm).

that for $e = 1$ mm, and $\dot{m}_{\text{cond}}$ at the peak in condensation rate is significantly decreased.

Comparisons between the evolutions of the latent and sensible heat fluxes at one of the vertical cooled surface are shown in Fig. 7. As it can be seen, condensation heat transfer largely dominates over most of the transient regime. For larger times, the sharp decrease in $\bar{q}_w$ as a function of time corresponds to a fast reduction in the mass of water vapor in the cavity. When the mass fraction and temperature distributions approach their asymptotic values, both heat and mass transfer are mainly diffusive and the time required to reach the full steady state conditions is rather important, especially for the thickest wall. Plots of the time-variation of the mean temperatures of the cold surfaces show indeed that they are only $\overline{T}_w = 282$ K at $t \approx 400$ s for the $e = 1$ mm thick wall.

The temperature and mass fraction distributions together with the streamlines are displayed in Fig. 8 for various typical times. The perfect symmetry of the flow fields about the vertical middle plane are evidenced during the transient regime. At $t = 20$ s, the mass fraction is uniform and pure thermal convection leads to a vertical temperature stratification within the cavity core with the lowest temperatures along the bottom wall. At $t = 50$ s, solutal convection dominates (see Fig. 7) and the changes in the shapes of the isotherms and streamlines are the result of thermosolutal convection. At $t = 300$ s, the mass fraction of water vapor has been reduced by an order of magnitude and tends towards the uniform steady-state value $W_v = 0.0095$ (Table 4). At larger times, the fluid motion is thermally driven, as at early times. The following energy balance must then be satisfied between the initial and steady states:

$$\Delta E_{\text{total}} = \Delta E_{\text{cond}} + \Delta E_{\text{walls}} + \Delta E_{\text{mixture}} \tag{23}$$

The left-hand side term in Eq. (23) stands for the amount of heat transferred to the ambient throughout the entire time evolution. The first term of the right-hand side in Eq. (23) is for energy due to condensation, the second and third terms account for the decreases in internal energy of the solid walls and ideal gas mixture. Since the mass of dry air is constant and by assuming temperature-independent properties of the solid walls, Eq. (23) can be rewritten as:

$$\begin{cases} 2\displaystyle\int_0^{\infty}\int_0^{H} h_{cv}\big(T_s(D+e,y,t)-T_\infty\big)\,\mathrm{d}y\,\mathrm{d}t \\ \quad = 2\displaystyle\int_0^{\infty}\int_0^{H} \frac{\rho_m D_{v,m} h_{lv}(T)}{1-W_{v,1}} \left.\frac{\partial W_v}{\partial x}\right|_{x=D} \mathrm{d}y\,\mathrm{d}t \\ \quad + 2m_s C_{ps}(T_0 - T_\infty) \\ \quad + \left[m_a \displaystyle\int_{T_0}^{T_\infty} \left(C_{p,a} - \frac{R}{M_a} \right) \mathrm{d}T \right. \\ \quad \left. + \frac{V M_v}{R} \displaystyle\int_{T_0}^{T_\infty} \frac{P_v}{T} \left(C_{p,v} - \frac{R}{M_v} \right) \mathrm{d}T \right] \end{cases} \tag{24}$$

Approximate hand-calculations of the decrease in internal energy of the gas mixture based on Eq. (24) are given in Appendix A. These calculations were conducted by assuming a constant value of the latent heat and a linear variation with temperature of the vapor pressure between the initial and steady states. The thermodynamic vapor pressure data displayed in

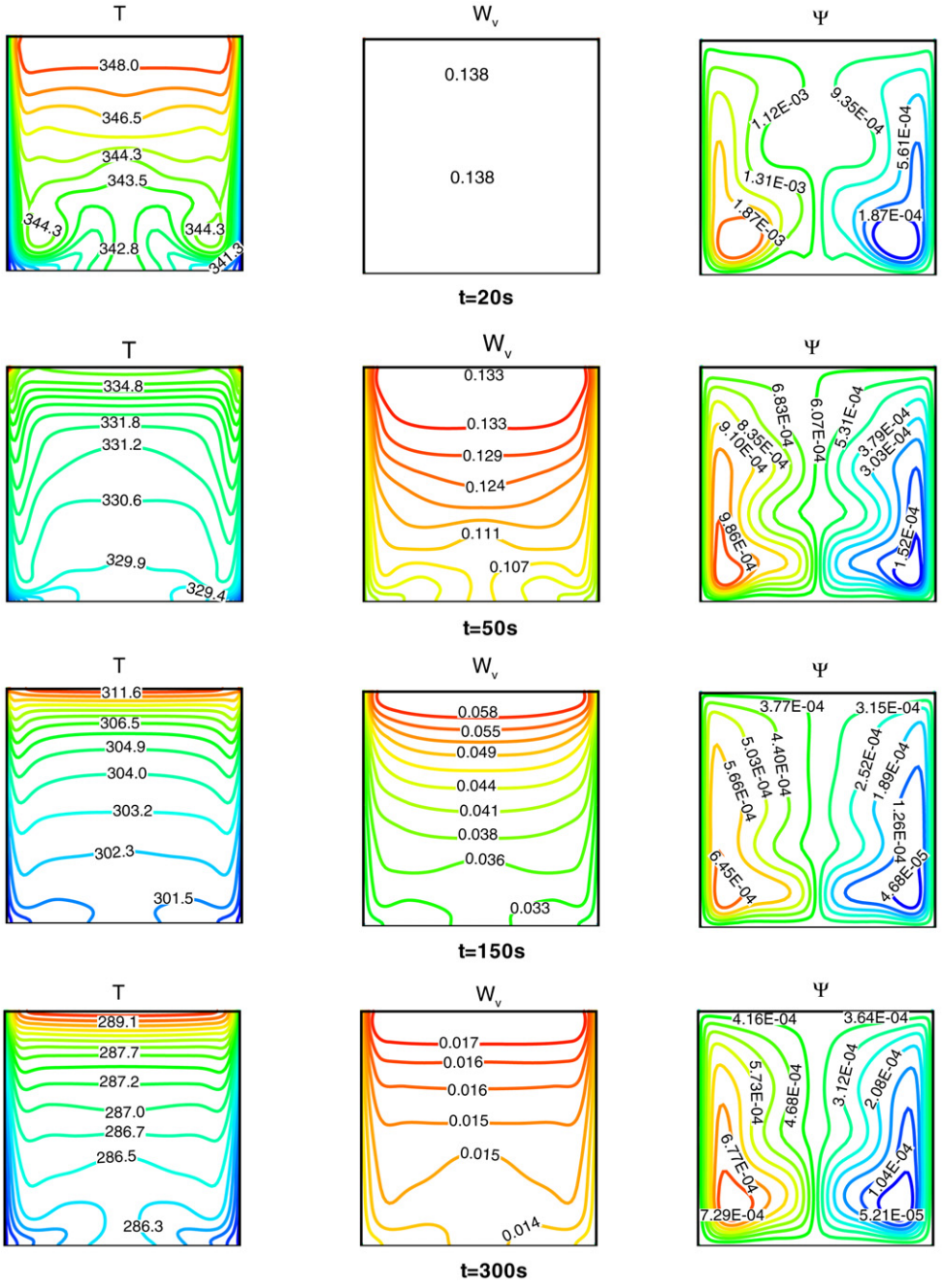

Fig. 8. Isotherms, isolines of mass fraction and streamlines for $e = 1$ mm.

Table 5
Comparisons between computed internal energy loss ($\Delta E_{\text{computed}}$) and thermodynamic approximate calculations (ΔE_{total} based on Eq. (24))

e (mm)	m_{cond} (g m^{-1})	$\Delta E^{(1)}_{\text{computed}}$ (J)	ΔE_{walls} (J)	$\Delta E_{\text{mixture}}$ (J)	ΔE_{cond} (J)	$\Delta E^{(2)}_{\text{total}}$ (J)	$\frac{(1)-(2)}{(2)}$
1	4.86	81,548	68,519	1834	11, 688	82,041	0.60%
3	4.86	218,622	205,554	1834	11, 688	219,076	0.21%

Table 4 and the temperature variations of $C_{p,a}$ and $C_{p,v}$ reported in Appendix A were used. Comparisons between these approximate calculations and time-integration of the heat flux balance given by Eq. (18) are reported in Table 5. As can be seen, the agreement is satisfied within less than 0.6%. The numerical computations show that contribution of phase change dominates largely over those due to heat diffusion and species interdiffusion (first and second terms in the right-hand side of Eq. (18)).

Further insight into the effect of species interdiffusion was gained by comparing the results with those obtained by neglecting interdiffusion since rather large variations in the Lewis

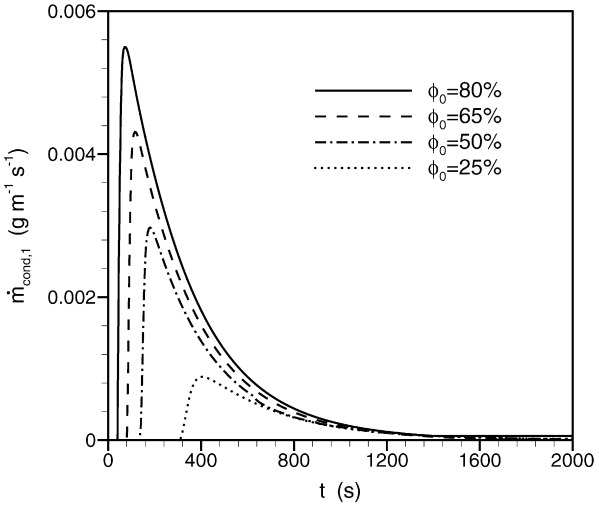

Fig. 9. Variation of the mass flow rate of water vapor condensed at the cold surface according to the initial relative humidity in the differentially heated cavity.

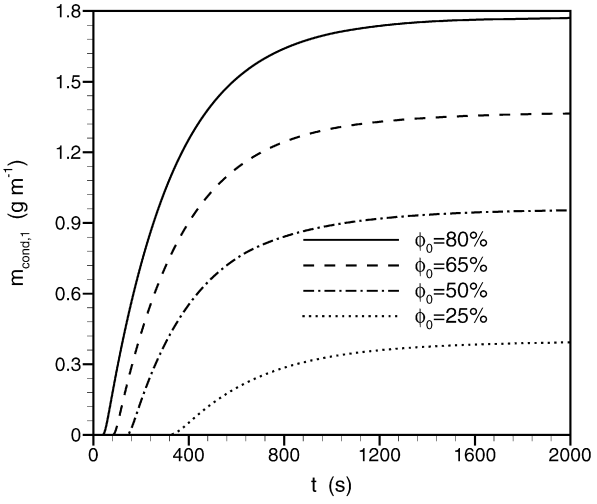

Fig. 10. Variation of the mass of water vapor condensed at the cold surface for various initial relative humidities in the differentially heated cavity.

number could occur between the initial and steady states according to the initial relative humidity. The comparisons of time heat flux evolutions at the inner wall-surfaces showed negligibly small differences for the cases investigated because the mixtures were largely composed of dry air. In addition, the mixture internal energy losses by sensible and latent heat differ by less than one percent when the effect of species interdiffusion is accounted for. In conclusion, it can be assumed that the interdiffusion contribution is small.

4.3. Thermosolutal convection in a differentially heated cavity

Transient thermosolutal convection of humid air within a square cavity having a hot wall at uniform temperature $T_h = 350$ K and a bounding wall of finite thickness suddenly put in contact with a cold ambience at $T_\infty = 280$ K is considered in this section. The initial conditions were for humid air at rest ($T_0 = T_h = 350$ K). All of the computations were for a 0.1 m-width cavity bounded by a 10^{-3} m glass sheet ($\rho_s = 2500\ \mathrm{kg\,m^{-3}}$, $C_{ps} = 1000\ \mathrm{J\,kg^{-1}\,K^{-1}}$, $k_s = 1\ \mathrm{W\,m^{-1}\,K^{-1}}$). The problem parameters are thus the initial relative humidity ϕ_0 and the external heat transfer coefficient h_{cv}.

First, the external heat transfer coefficient was maintained at $h_{cv} = 5\ \mathrm{W\,m^{-2}\,K^{-1}}$ while the initial relative humidity was varying between $\phi_0 = 25\%$ and 80%. Second, the heat transfer coefficient was increased up to $h_{cv} = 30\ \mathrm{W\,m^{-2}\,K^{-1}}$ while the initial relative humidity was kept at $\phi_0 = 80\%$.

4.3.1. Effects of the initial relative humidity

Figs. 9 and 10 show the time-variations of the water vapor mass flux rates and mass condensed at the cold inner surface as a function of time according to various values of the initial relative humidity. Obviously, condensation occurs as soon as the temperature at the coolest part of the inner surface of the bounding wall falls below the dew-point temperature. Therefore, the elapsed time at which the fluid motion is only due to thermal convection extends over a period inversely proportional to the

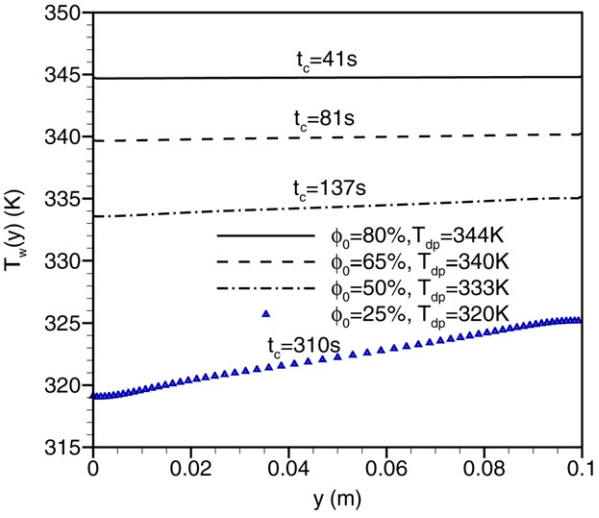

Fig. 11. Temperature distributions at the cold surface in the presence of condensation for various ϕ_0.

value of the initial relative humidity: it increases from about 41 s to about 310 s in the range of ϕ_0 considered. The transient variation of the water–vapor mass condensed depends strongly on ϕ_0, as it is clearly shown in Figs. 9 and 10.

Temperature distributions along the cooled inner surface are shown in Fig. 11 at time-values corresponding to the beginning of condensation for the various initial relative humidities. For the highest initial relative humidity, condensation occurs while the temperature of the cooled surface is almost uniform. On the other hand, a noticeable thermal vertical gradient exists when condensation starts from $\phi_0 = 25\%$. These temperature distributions reveal that a significant thermal convective flow exists at the beginning of condensation for the smallest values of ϕ_0 while it starts from a purely diffusive regime at the highest values. It can be thus concluded that the cold surface is almost uniformly wet at the beginning of condensation for $\phi_0 = 80\%$ while it is bottom wet for $\phi_0 = 25\%$. This conclusion can be deduced from the values of the dew-point temperature (T_{dp}) re-

ported in Fig. 11. Time variations of the averaged temperature of the cold surface displayed in Fig. 12 show higher temperatures with increases in ϕ_0 for about $\Delta t = 700$ s while the opposite is observed for t larger than ≈ 700 s. The explanation lies in the large heat flux associated with condensation. As it was emphasized previously, the phase change effects dominate when a significant mass flow rate of water vapor condensates and, then decrease after the condensation peak (Fig. 13). In the case $\phi_0 = 80\%$, the thermal effects are predominant when

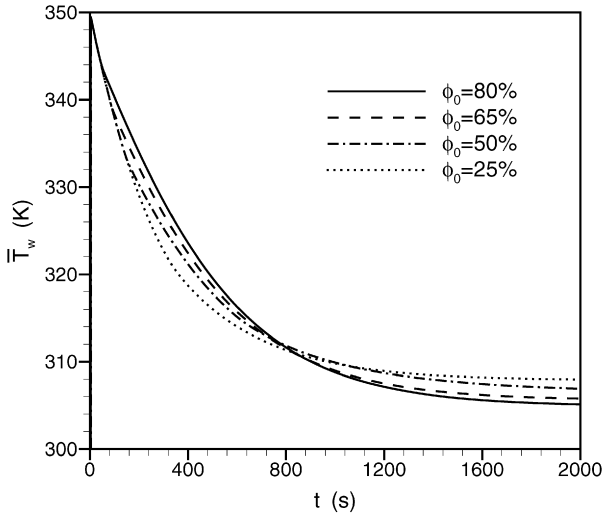

Fig. 12. Time variation of the averaged temperature of the cold surface according to ϕ_0.

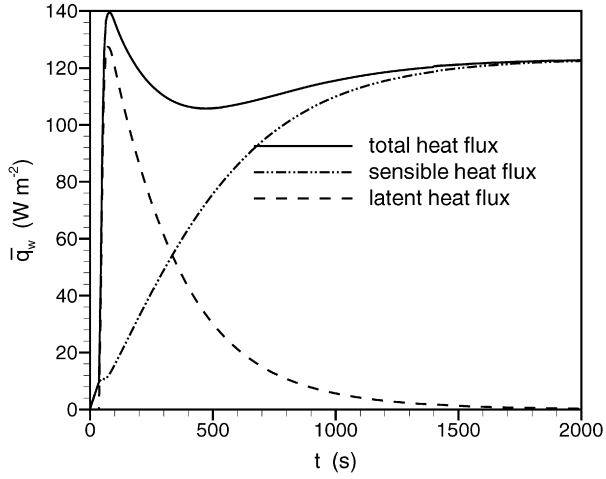

Fig. 13. Comparison between the latent and sensible heat fluxes for $\phi_0 = 80\%$.

$t \gtrapprox 400$ s because the mass fraction of water vapor becomes less than 0.1. The effective thermal Rayleigh number, Ra_T, based on the temperature difference $(T_h - \overline{T}_w(t))$ and volume averaged thermophysical properties of the mixture, is larger for the small ϕ_0-values. Therefore, thermal convection at steady-state is all the more significant since the initial relative humidity is low.

This result is supported by the values of transient thermal and solutal Rayleigh numbers reported in Table 6 for the cases investigated. In Table 6, t_c denotes the time at which condensation starts to occur (see Fig. 10). At t_c, the thermal Rayleigh number is much higher for $\phi_0 = 25\%$ than for $\phi_0 = 80\%$, mainly because of the larger temperature differences between the hot and cold walls. At $t = 2000$ s (i.e. steady state), the differences in Ra_T reflects chiefly the effect of decrease in mixture density since the other thermophysical properties are almost independent of ϕ_0. The solutal Rayleigh numbers are of two or three orders of magnitude smaller than the thermal Rayleigh numbers during the transient regime. Invoking the Boussinesq approximation and ideal gas equation of state, the buoyancy parameter, $N = Ra_M/Ra_T$, based on average properties is always positive during the transient regime (solutal and thermal buoyancy forces are augmenting) but decreases from the onset of condensation (i.e. $t = t_c$ in Table 6) to steady state. For example, N decreases from 0.036 at $t = t_c$ to $6.0 \cdot 10^{-4}$ at steady state for $\phi_0 = 80\%$. Obviously, the importance of solutal force is more important for large initial relative humidity. It can be thus concluded that convection is thermally driven for all of the cases considered.

The computations were carried out by using a compressible flow model. To justify this mathematical formulation, it is therefore relevant to examine the time-changes in averaged density or thermodynamic pressure. Since the mixture is assumed to be a perfect gas at constant volume, evolutions of density and pressure are almost similar. Due to space limitations, the density changes for the various ϕ_0 considered is plotted only (Fig. 14). The reference curve is that for dry air ($\phi_0 = 0\%$) for which the Boussinesq model is almost valid on account of the possible maximal temperature difference ($T_h - T_\infty = 70$ K): the density is constant while the decrease in thermodynamic pressure follows the decrease in averaged volume temperature of the mixture. Each of the density curves exhibits a plateau at early times. It means that condensation has not started. The time lengths of the plateau are those reported in Fig. 10. The decreases in density are larger for higher ϕ_0 and the steady-state values are smaller. Since the steady-state volume averaged temperature of the mixture depends weakly on ϕ_0 for a given h_{cv},

Table 6
Thermal and solutal Rayleigh numbers based on volume averaged properties at various times and, maximum value of the buoyancy parameter (t_c denotes the time (s) for the onset of condensation as shown in Figs. 10 and 11)

ϕ_0 (%)	Ra_T			Ra_M			N_{max}
	t_c	$t = 400$ s	$t = 2000$ s	t_c	$t = 400$ s	$t = 2000$ s	
25	$1.509 \cdot 10^6$	$1.682 \cdot 10^6$	$2.123 \cdot 10^6$	$1.061 \cdot 10^3$	$3.144 \cdot 10^3$	$9.685 \cdot 10^2$	$0.7 \cdot 10^{-3}$
50	$8.750 \cdot 10^5$	$1.348 \cdot 10^6$	$1.797 \cdot 10^6$	$1.072 \cdot 10^3$	$6.469 \cdot 10^3$	$7.929 \cdot 10^2$	$1.2 \cdot 10^{-3}$
65	$5.694 \cdot 10^5$	$1.138 \cdot 10^6$	$1.557 \cdot 10^6$	$1.085 \cdot 10^3$	$9.516 \cdot 10^3$	$6.755 \cdot 10^2$	$1.9 \cdot 10^{-3}$
80	$3.018 \cdot 10^5$	$9.540 \cdot 10^5$	$1.340 \cdot 10^6$	$1.103 \cdot 10^4$	$1.271 \cdot 10^4$	$5.726 \cdot 10^2$	$3.6 \cdot 10^{-2}$

the final thermodynamic pressure can be easily calculated: $\overline{P}_\infty$ decreases almost at the same rate as $\overline{\rho}_{m_\infty}$ as it can be seen from the initial and steady-state volume-averaged quantities reported in Table 7.

Fig. 15 illustrates the differences between transient flow fields for dry air and for humid air in the case $\phi_0 = 80\%$. The isotherms and isolines of relative humidity have similar shapes, especially over the regions of almost uniform W_v since hot air contains larger mass fractions of water vapor than cold air. On the other hand, relative humidity exhibits the lowest values along the hot wall and reaches 100% at the cold wall and in the bottom cold part of the cavity. Owing to the variations of properties with temperature and mass fraction, the isothermal patterns and streamlines do not verify the classical centrosymmetry property, even at early times for which the cold wall temperature is nearly uniform. The transient increase in the maximum value of streamfunction indicates augmentation in circulation caused by larger temperature gradients. At steady state, the buoyancy force due to solutal gradients is negligible as compared to the thermal body force over most of the cavity cross-section. The thermal boundary layer along the cold wall is much thicker than the solutal boundary layer and the two body forces are augmenting. The mixture density is indeed continuously increasing from the top to the bottom of the cold wall owing to decreases in temperature and increases in mass fraction of water vapor within the thermal boundary layer.

Cold surface temperature distributions for dry air and for the case $\phi_0 = 80\%$ are shown in Fig. 16 at various times following

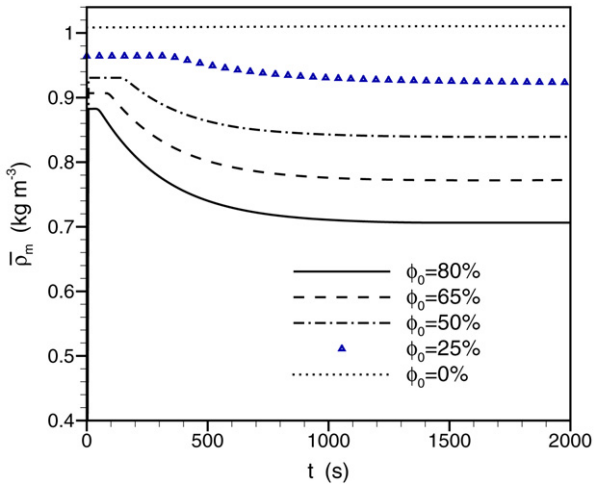

Fig. 14. Time variation of the volume averaged density for various ϕ_0.

the occurrence of condensation. At $t = 100$ s and $t = 300$ s, the temperatures corresponding to humid air are higher and more uniform since the latent heat flux predominates (see Fig. 13), although the thermal Rayleigh number is about two times larger for dry air. Reduction with time of the amount of water vapor present in the cavity and decrease in the cold wall temperature render then the thermal body force dominant, especially along the top part of the cold wall where condensation rate decreases more quickly. As a result, the temperature distribution for dry air at $t = 1200$ s shows an increase in vertical temperature gradient with higher top wall temperature due to the larger circulation rate as compared with humid air.

4.3.2. *Effects of the external heat transfer coefficient*

All the computations were carried out for a cavity initially filled with hot humid air at uniform temperature $T_0 = T_h = 350$ K and relative humidity $\phi_0 = 80\%$. Water vapor and mixture masses were $m_{v0} = 2.08$ g m^{-1} and $m_{m0} = 8.83$ g m^{-1} at $t = 0$, respectively. The external heat transfer coefficient was varied from $h_{cv} = 5$ W m^{-2} K^{-1} to $h_{cv} = 30$ W m^{-2} K^{-1}. Larger values of h_{cv} yield an almost uniform cold wall temperature of $T_\infty = 280$ K. On account of the thickness and thermal conductivity of the bounding wall, the Biot number based on h_{cv} was $Bi = 10^{-3} h_{cv}$. Obviously, the vertical temperature gradient along the cold surface was highest for the smallest value of h_{cv}.

Increases in the external heat transfer coefficient lead to decreases in the wall temperature and duration of the transient regime from about 2000 s to about 300 s for the range of h_{cv} considered. Consequently, the mass of water vapor condensed increases while the mixture density, average pressure and temperature are significantly reduced at steady state as it can be deduced from the data reported in Table 8. It can also readily shown that the average pressure (or thermodynamic pressure) agrees well with the state equation, as expected when the problem formulation is based on a low-Mach number formulation. The isocontours displayed in Fig. 17 (and Fig. 15 for $h_{cv} = 5$ W m^{-2} K^{-1}) do not show noticeable changes in the flow structure at steady-state. The explanation is that the thermal Rayleigh numbers are almost identical. Finally, in the range of h_{cv} considered, the most significant effect of h_{cv} is to produce a decrease in the time required to reach the steady-state regime at which water vapor mass fraction and relative humidity are the most different field variables according to the h_{cv}-value.

Table 7
Mass quantities and thermodynamic pressure (subscripts: 0 at $t = 0$, ∞ at steady-state)

ϕ_0 (%)	m_{v_0} (g m^{-1})	m_{m_0} (g m^{-1})	W_{v_0}	$\overline{W}_{v_\infty}$	m_{cond} (g m^{-1})	$\overline{\rho}_{m_\infty}$ (kg m^{-3})	$\overline{P}_\infty$ (Pa)
25	0.65	9.69	0.067	0.027	0.40	0.927	$8.88 \cdot 10^4$
50	1.30	9.30	0.138	0.039	0.97	0.834	$8.10 \cdot 10^4$
65	1.69	9.06	0.185	0.040	1.38	0.768	$7.47 \cdot 10^4$
80	2.08	8.83	0.235	0.042	1.78	0.706	$6.83 \cdot 10^4$

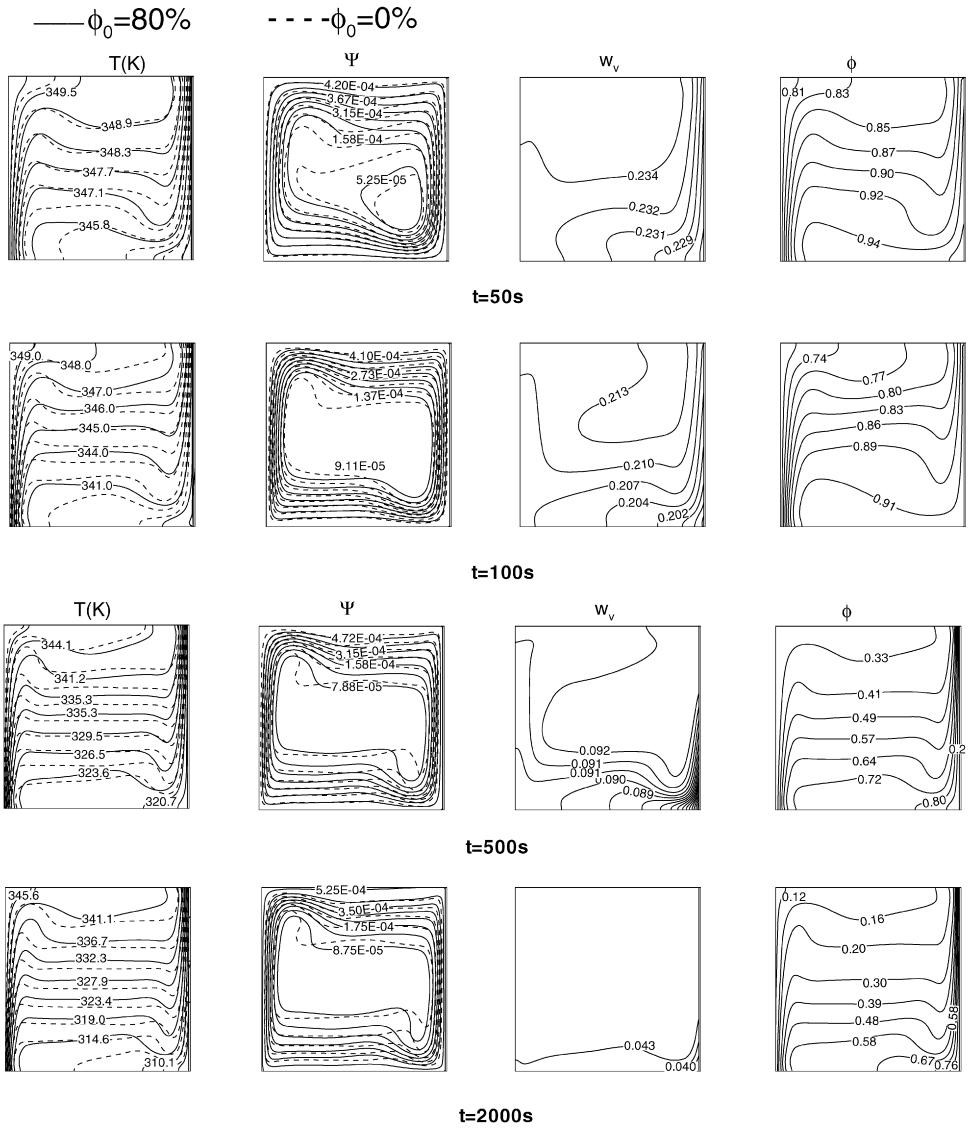

Fig. 15. Isotherms, streamlines, isolines of water vapor mass fraction and relative humidity at different times (dashed lines are for dry air) in the differentially heated cavity.

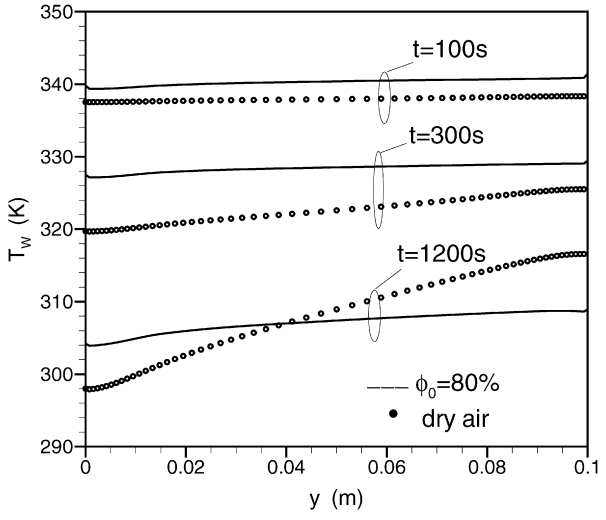

Fig. 16. Comparisons of the temperature distributions along the cold surface for dry air and humid air at various times.

5. Conclusions

A numerical study has been carried out to investigate buoyancy with induced heat and mass transfer of humid air in enclosures bounded by a wall of finite thickness in contact with a cold reservoir. The phase change problem formulation was based on the thin-film approximation and the flow of the liquid film was neglected. It has been shown that the usual incompressible-Boussinesq approximation is not relevant to handle the coupling of thermal and solutal forces. The transient effect associated with initial relative humidity on the heat and mass transfer was examined in detail for various boundary conditions. A brief summary of the major results is as follows:

1. When the Boussinesq approximation is not invoked, the steady-state regime depends on the initial conditions used, even for dry air and rather small temperature difference between the walls. Boussinesq and low Mach number solu-

Table 8
Effects of the external heat transfer coefficient h_{cv} on steady-state quantities

h_{cv} ($\mathrm{W\,m^{-2}\,K^{-1}}$)	$\overline{W}_{v_\infty}$	m_{cond} ($\mathrm{g\,m^{-1}}$) cooled surface	m_{cond_i} ($\mathrm{g\,m^{-1}}$) inner surfaces	$\overline{\rho}_{m_\infty}$ ($\mathrm{kg\,m^{-3}}$)	$\overline{P}_\infty$ (Pa)	$\overline{T}_\infty$ (K)
5	0.042	1.76	1.78	0.706	$6.83 \cdot 10^5$	327
10	0.027	1.87	1.88	0.695	$6.53 \cdot 10^5$	322
20	0.017	1.95	1.96	0.687	$6.36 \cdot 10^5$	319
30	0.013	1.98	1.99	0.683	$6.28 \cdot 10^4$	318

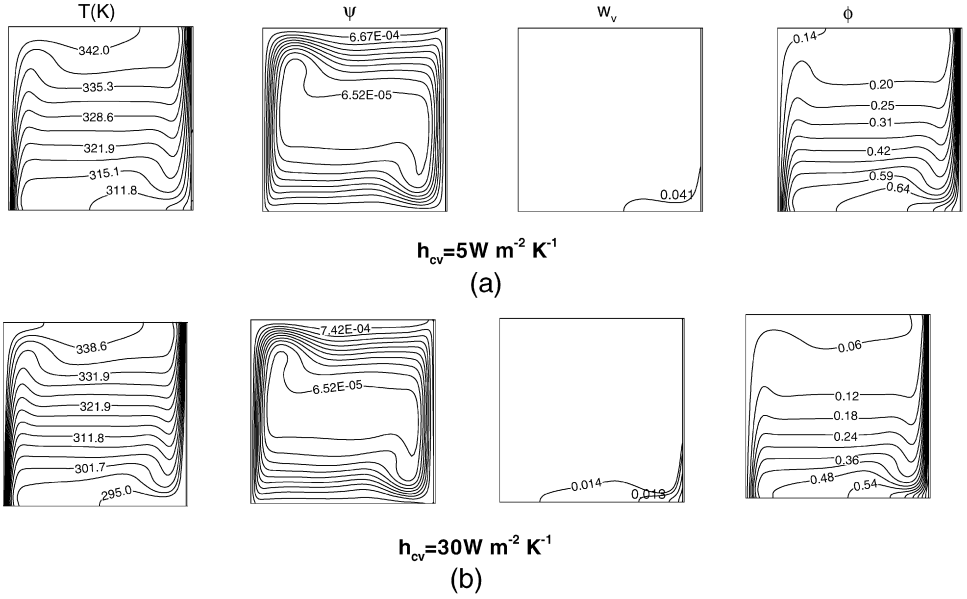

Fig. 17. Isotherms, streamlines, isolines of water vapor mass fraction and relative humidity at steady state for (a) $h_{cv} = 10\ \mathrm{W/m^2\,K}$ and (b) $h_{cv} = 30\ \mathrm{W/m^2\,K}$.

tions are close if the fluid is initially at uniform temperature to be the average of the wall temperatures.

2. High decreases in average pressure predicted by usual thermodynamic calculations are well recovered through transient resolutions of the flow, heat and mass conservation equations. The calculations allow well-based predictions of the evolutions shown in the heat and mass transfer regimes for condensation in a cavity initially filled with moist air and suddenly cooled at both vertical walls.
3. At the cold walls, the heat transfer regime consists generally of three periods: thermal, solutal and finally thermal-dominated heat transfer.
4. At the beginning of the transient regime in a differentially heated cavity, the temperatures of the wall of finite thickness in contact with a cold ambiance increase when surface condensation is accounted for.
5. On the other hand, when water vapor contained in the mixture is initially in sufficient amount, the decrease in fluid density compared to that for dry air leads to lower temperatures of the cooled wall of finite thickness at steady state, owing to decreases in thermal Rayleigh number.

Appendix A. Evaluation of thermophysical properties and internal energy change of humid air

We introduced in the computational code the properties of the components and those of the mixture given by Fujii et al. [18] (see also Yin et al. [7]).

The variations with temperature of the specific heat of the components were determined by the following relationships:

- Dry air:

$$C_{p,a} = 10^3 + 2.5 \cdot 10^{-7} T^3 \quad (\mathrm{J\,kg^{-1}\,K^{-1}}) \tag{A.1}$$

- Water vapor:

$$C_{p,v} = 1.863 \cdot 10^3 + 1.65 \cdot 10^{-3}(T - 273.16)^{2,5} + 1.2 \cdot 10^{-18}(T - 273.16)^{8,5} \quad (\mathrm{J\,kg^{-1}\,K^{-1}}) \tag{A.2}$$

- Latent heat of condensation ($\mathrm{J\,kg^{-1}}$) [22]:

$$h_{lv} = 2.5009 \cdot 10^3 \left(7.7922 \cdot 10^{-1} T_c^{1/3} + 4.6266 T_c^{5/6} - 1.0793 T_c^{7/8} + \sum_{i=1}^{i=6} S_i T_c^i \right) \tag{A.3}$$

with $T_c = \frac{647.3 - T}{647.3}$ (T in K) and

$$S_1 = 0; \quad S_2 = -3.87446; \quad S_3 = 2.94553;$$
$$S_4 = -8.06395; \quad S_5 = 11.5633; \quad S_6 = -6.02884$$

Between $T = 280$ K et $T = 350$ K, the change in latent heat of condensation ranges over $2316 \cdot 10^3\ \mathrm{J\,kg^{-1}} \leqslant h_{lv} \leqslant 2485 \cdot 10^3\ \mathrm{J\,kg^{-1}}$ (mean value $\overline{h}_{lv} = 2400 \cdot 10^3\ \mathrm{J\,kg^{-1}}$). The decrease

in the internal energy for an ideal mixture of diatomic gases as reported in Table 4 was calculated as:

$$\Delta E_{\text{mixture}} = \int_{T_0}^{T_\infty} m_a C_{v,a}\,\mathrm{d}T + \int_{T_0}^{T_\infty} m_v C_{v,v}\,\mathrm{d}T \tag{A.4}$$

Since dry air is incondensable, m_a is constant. Therefore

$$m_a C_{v,a} = m_a\left(C_p - \frac{R}{M_a}\right) \tag{A.5}$$

and

$$m_v C_{v,v} = m_v\left(C_p - \frac{R}{M_v}\right) = \frac{V P_v M_v}{RT}\left(C_p - \frac{R}{M_v}\right) \tag{A.6}$$

where $M_a = 28.966$ g/mol, $M_v = 18$ g/mol.

An approximate expression of the sum $(\Delta E_{\text{mixture}} + \Delta E_{\text{cond}})$ shown in Eq. (23) was obtained by assuming first that the enthalpy of condensation was equal to its mean value $\bar{h}_{lv} = 2400 \cdot 10^3\ \mathrm{J\,kg^{-1}}$ and, secondly that the partial pressure of water vapor was linearly varying between initial and steady states. P_v varying from 20,760 Pa at $T_0 = 350$ K to 990 Pa at $T_c = 280$ K (see Table 3), the linear relationship $P_v = 282.4T - 78082$ was used. Therefore

$$\begin{aligned}\Delta E_{\text{mixture}} + \Delta E_{\text{cond}} &= m_{\text{cond}}\bar{h}_{lv} + \left[m_a \int_{T_0}^{T_a}\left(C_{p,a} - \frac{R}{M_a}\right)\mathrm{d}T \right.\\ &\quad \left. + \frac{V M_v}{R}\int_{T_0}^{T_a}\frac{P_v}{T}\left(C_{p,v} - \frac{R}{M_v}\right)\mathrm{d}T\right]\end{aligned} \tag{A.7}$$

By using Eqs. (A.1) and (A.2), the last two terms may be rewritten as

$$m_a \int_{T_0}^{T_a}\left(C_{p,a} - \frac{R}{M_a}\right)\mathrm{d}T = m_a \int_{T_0}^{T_a}\left((1 + 2.5 \cdot 10^{-10}T^3)10^3 - \frac{R}{M_a}\right)\mathrm{d}T$$

and

$$\frac{V M_v}{R}\int_{T_0}^{T_a}\frac{P_v}{T}\left(C_{p,v} - \frac{R}{M_v}\right)\mathrm{d}T = \frac{V M_v}{R}\int_{T_0}^{T_a}\left(282.4 - \frac{78082}{T}\right)\left(C_{p,v} - \frac{R}{M_v}\right)\mathrm{d}T$$

The result is $\Delta E_{\text{mixture}} = 1542 + 292 = 1834$ J/m for a square cavity of dimensions 0.2 m × 0.2 m.

References

[1] J.A. Weaver, R. Viskanta, Natural convection due to horizontal temperature and concentration gradients. 1. Variable thermophysical properties effects, Int. J. Heat Mass Transfer 34 (12) (1991) 3107–3120.

[2] J.A. Weaver, R. Viskanta, Natural convection due to horizontal temperature and concentration gradients. 2. Species interdiffusion, Soret and Dufour effects, Int. J. Heat Mass Transfer 34 (12) (1991) 3121–3133.

[3] B. Gebhart, Y. Jaluria, R.L. Mahajan, B. Sammakia, Buoyancy-Induced Flows and Transport, Hemisphere Pub. Co., New York, 1988.

[4] A. Bejan, Convection Heat Transfer, third ed., John Wiley and Sons, New York, 2005.

[5] M.M. Rahman, M.J. Lampinen, Numerical study of natural convection from a vertical surface due to combined buoyancies, Numer. Heat Transfer Part A 28 (1995) 409–429.

[6] J. Chang, T.F. Lin, Transient natural convection heat and mass transfer over a vertical plate of finite height, Numer. Heat Transfer Part A 21 (1992) 187–214.

[7] T.F. Lin, C.J. Chang, W.M. Yan, Analysis of combined buoyancy effects of thermal and mass diffusion on laminar forced convection heat transfer in a vertical tube, ASME J. Heat Transfer 110 (1988) 337–344.

[8] W.M. Yan, Y.L. Tsay, T.F. Lin, Simultaneous heat and mass transfer in laminar mixed convection flows between vertical parallel plates with asymmetric heating, Int. J. Heat and Fluid Flow 10 (3) (1989) 262–269.

[9] K.T. Lee, H.L. Tsai, W.M. Yan, Mixed convection heat and mass transfer in vertical rectangular ducts, Int. J. Heat Mass Transfer 40 (7) (1997) 1621–1631.

[10] G. Desrayaud, G. Lauriat, Heat and mass transfer analogy for condensation of humid air in a vertical channel, Heat and Mass Transfer 37 (2001) 67–76.

[11] W.M. Yan, T.F. Lin, C.J. Chang, Combined heat and mass transfer in natural convection between vertical parallel plates, Wärme und Stoffübertragung 23 (1988) 69–76.

[12] J.A. Weaver, R. Viskanta, Natural convection in binary gases due to horizontal thermal and solutal gradients, ASME J. Heat Transfer 113 (1991) 140–147.

[13] Z. Rusak, J.C. Lee, Transonic flow of moist air around thin airfoil with non-equilibrium and homogeneous condensation, J. Fluid Mech. 403 (2000) 173–199.

[14] S.J. Karabelas, N.C. Markatos, Water vapor condensation in forced convection flow over an airfoil, Aerospace Science and Technology (2007), doi:10.1016/j.ast.2007.05.003.

[15] N. Schaeffer, F. Utheza, F. Garnier, G. Lauriat, Stable stratification alteration in a thermal diffusion cloud chamber, J. Chem. Phys. 113 (18) (2000) 8085–8092.

[16] S. Paolucci, On the filtering of sound from the Navier–Stokes equations, Technical report, Sandia National Laboratory, 1982, SAND82-8257.

[17] P. Le Quéré, C. Weisman, H. Pallière, J. Vierendeels, E. Dick, R. Becker, M. Braack, J. Locke, Modelling of natural convection flows with large temperature differences: A benchmark problem for low Mach number solvers. Part 1. References solutions, ESIAM, Math. Model. Numer. Anal. 39 (3) (2005) 609–616.

[18] T. Fujii, Y. Kato, K. Mihara, Expressions of transport and thermodynamic properties of air, steam and water, Sei San Ka Gaku Ken Kyu Jo, Report No. 66, Kyu Shu University, Kyu Shu, Japan, 1977.

[19] Fluent 6.2 User's Guide (n.d.), www.fluentusers.com.

[20] J.H. Ferziger, M. Perić, Computational Methods for Fluid Dynamics, second ed., Springer, 1999.

[21] P. Le Quéré, C. Weisman, H. Pallière, J. Vierendeels, E. Dick, R. Becker, M. Braack, J. Locke, Modelling of natural convection flows with large temperature differences: A benchmark problem for low Mach number solvers. Part 2. Contributions to the June 2004 Conference, ESIAM, Math. Model. Numer. Anal. 39 (3) (2005) 617–621.

[22] W.G. Reynolds, Thermodynamic properties in SI, graph, tables and computational equation for forty substances, Dept. of Mechanical Engineering Stanford University, 1979.